ACS APPLIED MATERIALS & INTERFACES

Research Article

www.acsami.org

Highly Textured FeCo Thin Films Deposited by Low Temperature Pulsed Laser Deposition

Gaspare Varvaro,[†] Davide Peddis,[†] Gianni Barucca,[‡] Paolo Mengucci,[‡] Valeria Rodionova,[§,∥] Ksenia Chichay,[§] Alberto Maria Testa,[†] Elisabetta Agostinelli,[†] and Sara Laureti*[,†]

[†]Istituto di Struttura della Materia, CNR, Monterotondo Stazione, Roma 00015, Italy

[‡]Università Politecnica delle Marche, Dipartimento SIMAU, Via Brecce Bianche, Ancona 60131, Italy

[§]Innovation Park and Institute of Physics and Technology, Immanuel Kant Baltic Federal University, Kaliningrad 238300, Russian Federation

[∥]National University of Science and Technology "MISiS", Moscow 119049, Russia

ABSTRACT: The effect of the deposition temperature (T_{dep}) on the crystallographic orientation of pulsed laser-deposited FeCo/MgO(100) thin film was determined by means of X-ray reflectivity and high resolution trasmission electron microscopy analysis and was correlated with the magnetic anisotropy properties measured by angle dependent hysteresis loops. Highly textured films with a bcc structure and very smooth surface were obtained even at room temperature, the film being [100] and [110] oriented, at T_{dep} = 25 °C and 150 °C, respectively. The cubic symmetry is reflected in the angular dependence of remanent magnetization, showing a 4-fold character, whose in-plane distribution is consistent with the different crystallographic orientations of the films. The high structural quality, even at room temperature, is reflected in a high value of the saturation magnetization and low coercivity, matching the requirements for technological applications.

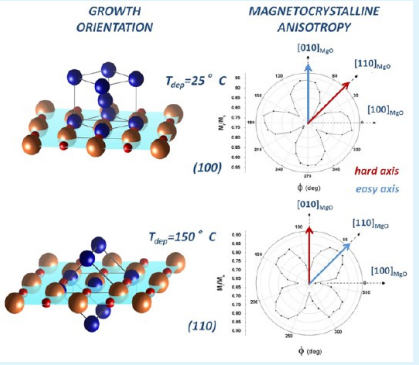

KEYWORDS: *FeCo, pulsed laser deposition, cubic magnetocrystalline anisotropy, growth orientation, thin films, ferromagnetic materials*

INTRODUCTION

Nowadays, the wide number of technological applications of magnetic materials requires not only strict control of their chemical and physical properties but also an always increasing capability to properly tailor their magnetic properties to optimize the devices performance. Among the ferromagnetic materials, the FeCo alloy is one of the most studied for its peculiar combination of high saturation magnetization (1.95 MA/m), high Curie temperature (1250 K), high permeability (up to 5000), and good mechanical properties,[1,2] providing high versatility and the ability to use this material in different applications. The soft ferromagnetic FeCo-based alloys are currently considered as the best candidate for spintronic-based devices (e.g., hard disk drive heads and magnetic random access memories)[3−5] because they allow for achieving the highest tunnelling magnetoresistance (TMR) value in highly oriented and crystalline FeCo(B)/MgO/FeCo(B) junctions.[6,7] Soft FeCo alloys have also been proposed in conjunction with hard magnetic materials, such as the $L1_0$-FePt alloy (exchange-coupled composite systems), for ultrahigh density magnetic recording media, which showed improved properties[8] with respect to the more commonly investigated Fe/FePt system[9−11] due to the larger value of saturation magnetization of the FeCo phase. The concept of an FeCo-based exchange-coupled system has also been envisaged for a novel permanent magnet exceeding the $(BH)_{max}$ value of NdFeB alloys while reducing the content of the critical and expensive rare-earth elements. Furthermore, it has recently been demonstrated both theoretically[12] and experimentally[13] that a highly anisotropic FeCo phase (K_u up to 10^7 J/m^3) can be obtained by properly tuning the FeCo chemical composition and tetragonal distortion, this material being of great interest for the previously mentioned applications.

In other words, the rich phase diagram that arises from the full miscibility of the two elements in the whole concentration range makes the FeCo a peculiar system whose magnetic properties can be suitably tailored, providing that precise control over the stoichiometry and the structure is ensured.[14,15] For this purpose, the choice of the fabrication process is of crucial importance, especially when the structural order is required over a restricted thickness or volume, i.e., in nanostructured thin films and nanoparticles.

Among the deposition techniques to produce thin films, pulsed laser deposition (PLD) has the peculiarity of growing materials from a plasma formed by high energy species (with kinetic energies E_k between 10 and 100 eV), resulting in an enhanced surface mobility of the adatoms that settle on the substrate,[16,17] thus leading to smooth film surfaces and high

Received: July 8, 2015
Accepted: September 17, 2015
Published: September 17, 2015

DOI: 10.1021/acsami.5b06030
ACS Appl. Mater. Interfaces 2015, 7, 22341−22347

crystallographic quality. Moreover, the laser source is outside the vacuum chamber, and this provides a much larger flexibility in the choice of the material as a target, the geometrical arrangements, and the variation of the deposition parameters. Thanks to the congruent removal of the target constituents, PLD has been widely used to deposit complex metal oxide films, such as high-Tc superconductors, hexaferrites, and multiferroics.[17,18] Furthermore, in the last few decades, this technique has been successfully exploited for the growth of metallic thin films and multilayers,[19−24] paving the way for a simpler process to fabricate a new class of advanced multifunctional films and heterostructures (i.e., ferroelectric/ferromagnetic materials) where complex oxides and metallic alloys are properly combined.

In this paper, we demonstrate that, by properly choosing the laser fluence, temperature, and substrate, it is possible to obtain high quality continuous $Fe_{50}Co_{50}$ thin films on MgO (100) substrates characterized by low coercivity, high saturation magnetization, and a high degree of crystallographic order even at 25 °C, and with the possibility to vary the growth orientation by slightly changing the substrate temperature. The high instantaneous deposition rate caused by the high laser energy fluence in a short pulse duration (17 ns) and the low temperature of the substrate are considered key parameters affecting the film growth mechanism and the relative orientation with respect to the MgO (100) plane.

EXPERIMENTAL SECTION

Continuous $Fe_{50}Co_{50}$ films were deposited on polished MgO (100) single-crystal substrates (Crystal) at 25 and 150 °C deposition temperature (T_{dep}) in a high vacuum PLD chamber. Hereafter, the samples will be denoted according to T_{dep} (i.e., S25 and S150). Depositions were performed by focusing a pulsed KrF excimer laser (λ = 248 nm, pulse duration = 17 ns) with a spot energy fluence of 7 J/cm^2 on a rotating FeCo target made of two equal sectors of the individual elements (purity of 99.99%) assembled to form a 2 cm diameter disk; the high rotation speed of ∼1000 rpm ensures the homogeneity of the deposited material on the substrate, which is assembled in a frontal geometry at 50 mm from the target. The PLD chamber was evacuated down to a base pressure of 5×10^{-7} mbar prior to the film deposition. The laser pulse repetition rate was 10 Hz for a deposition duration of 10 min, leading to a film thickness of ∼14 nm. To protect the samples against oxidation, a thin Cu capping layer was deposited on top. The final alloy composition was determined by means of energy dispersive X-ray spectrometry (EDS) analysis performed by a Zeiss Supra 40 field emission scanning electron microscope (FESEM) equipped with Bruker Quantax 200 micro-analysis, which confirmed a Co/Fe ratio close to 1.

To obtain information about the thickness, surface roughness, and density of the deposited layers, we carried out X-ray reflectivity (XRR) measurements using a Bruker D8 Advanced diffractometer equipped with a θ–θ goniometer. The XRR analyses were performed using Cu Kα radiation, and the obtained data were fitted by the Leptos 3.03 (Bruker AXS GmbH) simulation software.

The structural characterization was carried out by transmission electron microscopy (TEM) using a Philips CM200 microscope operating at 200 kV and equipped with an LaB6 filament. For TEM cross-sectional observations, samples were prepared by the conventional thinning procedure consisting of mechanical polishing by grinding papers, diamond pastes, and a dimple grinder. Final thinning was carried out by an ion beam system (Gatan PIPS) using Ar ions at 5 kV.

The magnetic properties were studied at room temperature using a commercial vector vibrating sample magnetometer (VSM model 10, ADE Technologies) equipped with a rotating electromagnet. The direction of magnetization with respect to the applied magnetic field was determined by measuring in-plane hysteresis loops at different angles in the film plane. Each loop was corrected for the diamagnetic substrate and sample holder contributions.

RESULTS

Figure 1 reports the experimental XRR curves of the two samples (open dots) superimposed to the simulated data fitting

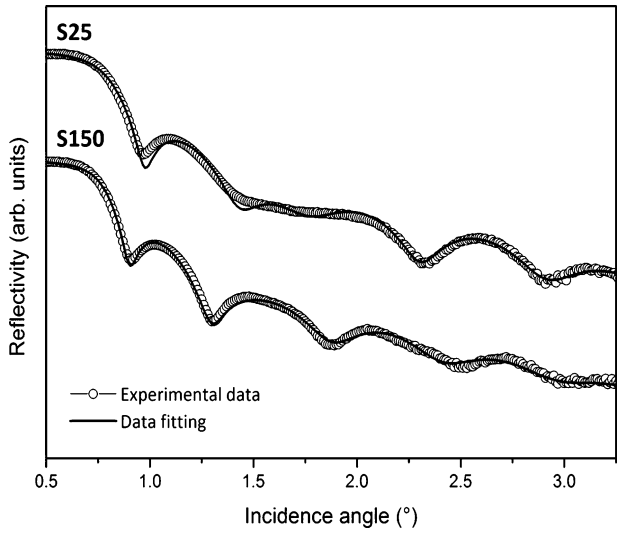

Figure 1. XRR curves of samples S25 and S150.

(continuous line). The simulation was carried out considering each sample as constituted of two separate continuous layers (i.e., FeCo and Cu) with sharp interfaces deposited on the MgO substrate. From the figure, it is evident that the data fitting are in close agreement with the experimental data for both curves, indicating reliable quantitative results (Table 1).

Table 1. Results of the XRR Experimental Data Simulation: Thickness (t), Roughness (σ), Calculated Density (ρ_c), and Nominal Bulk Density (ρ_n)[a]

sample	material	t (nm)	σ (nm)	ρ_c (g/cm^3)	ρ_n (g/cm^3)
S25	Cu	3.0 ± 0.9	1.3 ± 0.2	4.8 ± 0.8	8.935
	FeCo	12.5 ± 0.3	1.0 ± 0.2	7.1 ± 0.3	8.173
	MgO		0.50 ± 0.09	3.5698	3.5698
S150	Cu	2.8 ± 0.9	2.2 ± 0.5	5.9 ± 0.7	8.935
	FeCo	15.1 ± 0.4	1.0 ± 0.3	7.0 ± 0.2	8.173
	MgO		0.46 ± 0.08	3.5698	3.5698

[a]The uncertainties associated with each parameter are the standard deviations provided by the Leptos simulation program.

It is worth noting that the value of the nominal density ρ_n of the FeCo magnetic layer corresponds to the density of the cubic FeCo (Wairauite) stable compound (ICDD card no. 44-1433). This value was used as the initial density value of the FeCo layer in the simulation program. The results reported in Table 1 show that the two samples are almost identical, being the measured thickness very close to the nominal one. The only detectable differences are a slightly thicker magnetic layer and a slightly higher surface roughness of the Cu layer for sample S150.

TEM bright field images of the two samples are shown in Figure 2. The magnetic layers are continuous with a low roughness and a uniform thickness of (12.0 ± 0.5) nm and (16 ± 1) nm for the S25 and S150 samples, respectively, these

DOI: 10.1021/acsami.5b06030
ACS Appl. Mater. Interfaces 2015, 7, 22341−22347

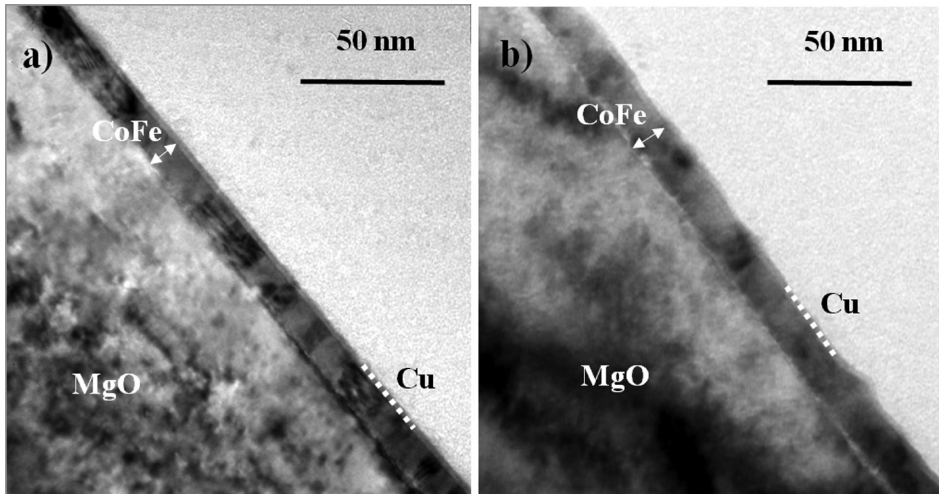

Figure 2. Bright field TEM images of samples S25 (a) and S150 (b).

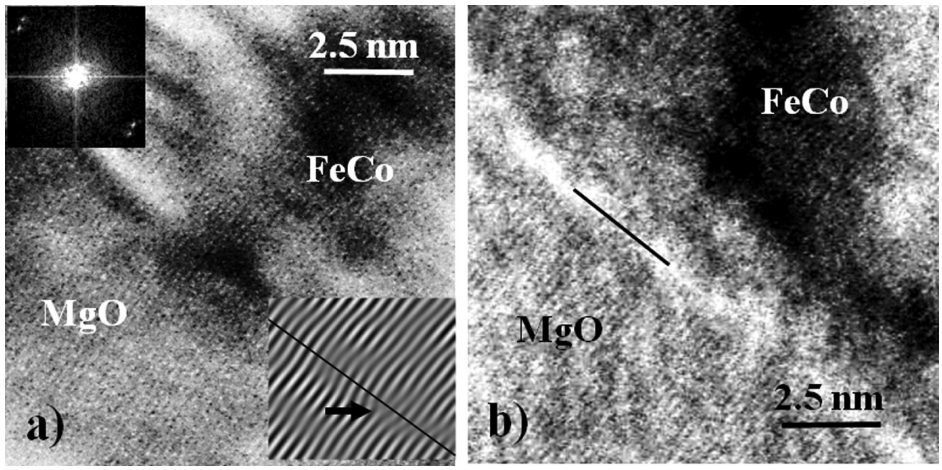

Figure 3. HR-TEM images of (a) S25 and (b) S150. The interface between the substrate and the magnetic layer is indicated by a dark line. The insets of (a) are an FFT of the image (upper) and a reconstructed image of the interface (lower) of the image, respectively.

values being in perfect agreement with the XRR data. Although the deposition parameters, which mainly affect the film thickness (deposition time and laser fluence) were fixed for both samples, such a difference may be considered within the limit of reproducibility of the PLD process, which is highly directional and consequently extremely sensitive to the plume-to-substrate reciprocal position and angle. The copper overlayer is continuous and ∼2 nm thick. The magnetic layers are crystalline and composed of columnar grains (Figure 2), the lateral size of the grains ranging between 4 and 12 nm for sample S25 (Figure 2a) and between 5 and 15 nm for sample S150 (Figure 2b).

The crystallinity of the magnetic layers is confirmed by the high-resolution TEM (HR-TEM) images reported in Figure 3.

In both samples, two families of lattice planes are visible corresponding to the substrate and the magnetic layer. The lattice planes of the substrate are perpendicular to the interface, and their interplanar distance of 0.210 nm is compatible with the MgO {200} planes. The lattice planes in the FeCo layer are slightly tilted with respect to the interface normal and have an interplanar distance of 0.200 nm, compatible with the FeCo {110} planes (considering the body centered cubic (bcc) structure of FeCo).

The upper inset of Figure 3a reports the fast Fourier transform (FFT) of the entire corresponding image. A similar FFT is obtained for the whole image of the sample deposited at higher temperature. In the upper inset of Figure 3a, the two visible spots at the upper left and bottom right corners are due to the previously mentioned MgO {200} and FeCo {110} planes. The distance of the spots from the center depends on the interplanar distance of each set of planes, and their angular separation confirms the slightly different inclination of the MgO and FeCo lattice planes with respect to the interface normal. A portion of the inverse FFT of the image, obtained using only the couple of spots visible in the FFT, is reported in the lower inset of Figure 3a. This image is evidence of the continuity of the lattice planes from the substrate to the magnetic layer. However, taking into account the different interplanar distance values of the two sets of lattice planes (0.210 nm for MgO and 0.200 nm for FeCo), the formation of dislocations at the interface between the substrate and the magnetic layer is predictable. The presence of a dislocation at the interface between MgO and FeCo in the S25 sample is clearly visible in the lower inset of Figure 3a (arrow); on the contrary, in the S150 sample (Figure 3b), the interface between the substrate and the magnetic layer is disordered, and a clear

DOI: 10.1021/acsami.5b06030
ACS Appl. Mater. Interfaces 2015, 7, 22341−22347

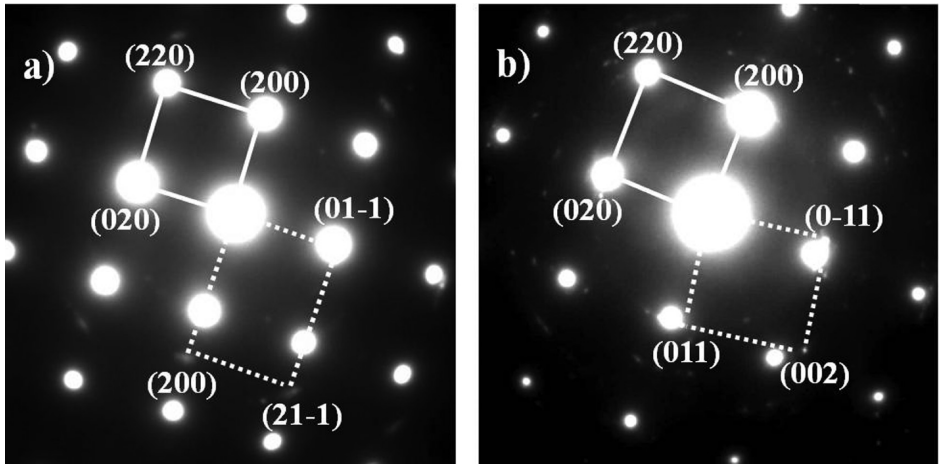

Figure 4. SAED patterns of sample S25 (a) and S150 (b). The MgO cell in orientation [001] is indicated by continuous lines, whereas the FeCo cells in orientation [011] (S25) and [100] (S150) are indicated by dashed lines.

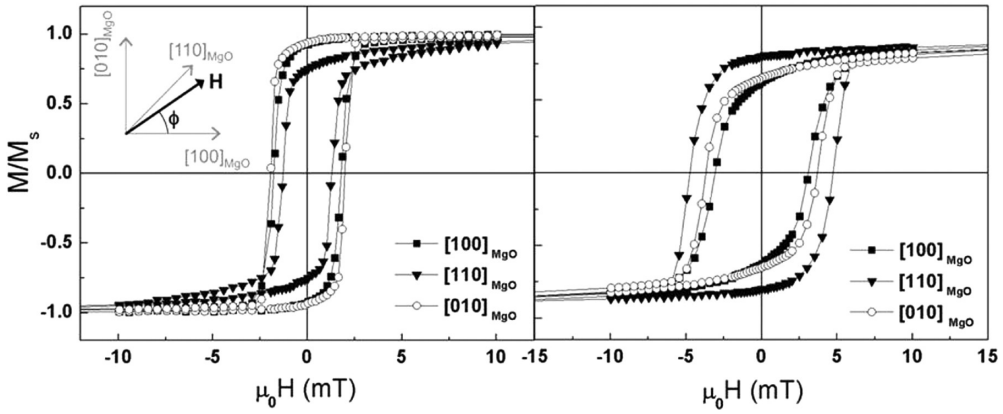

Figure 5. Room temperature hysteresis loops measured along the [100], [110], and [010] in-plane MgO crystallographic orientations of sample S25 (left) and sample S150 (right).

continuity of the lattice planes from one side to the other of the interface is not visible.

To identify the crystallographic structure of the magnetic layers, we carried out selected area electron diffraction (SAED) measurements on the two samples. A selected area aperture corresponding to a circular area of 300 nm diameter on the sample was used to record the SAED patterns. The sample was positioned with the deposited film corresponding to a diameter of the circular aperture. Because of the aperture size, the SAED patterns contain information from both the substrate and the deposited film.

Typical SAED patterns are shown in Figure 4a and b for samples S25 and S150, respectively.

Figure 4a shows intense diffraction spots due to the MgO substrate in the <001> zone axis orientation (continuous cell) and low intensity regularly distributed spots that can be attributed to the FeCo film (dashed cell). From the interplanar distances associated with these last diffraction spots and their distribution, it is possible to deduce that the FeCo layer is in a body centered cubic (bcc) phase with a lattice parameter a = (0.286 ± 0.02) nm. Furthermore, the FeCo grains grew oriented with respect to the substrate with the following orientation relationships: {100}FeCo // {100}MgO ; <011> FeCo // <001> MgO. In sample S25 in particular, the CoFe grains grow with the {100} lattice planes parallel to the interface plane. Analyzing the SAED pattern of sample S150 (Figure 4b), the diffraction spots due to the MgO substrate oriented in the <001> zone axis are clearly visible (continuous cell). In this case, however, the most intense diffraction spots due to the FeCo layer are regularly distributed in a different way with respect to the previous sample (compare the dashed cells of Figure 4). Measuring the interplanar distances associated with the spots and their geometry, it is possible to deduce, again, that the FeCo is in a body centered cubic (bcc) phase with the same lattice parameter and orientation relationships with the substrate obtained for the sample deposited at room temperature. The only difference is that now the FeCo grains grow with the {011} lattice planes parallel to the interface plane. It is worth noting that, in this case, by a rotation of 90° around the normal to the interface plane, two equivalent orientations of the CoFe cell on the interface plane are possible (as also evidenced in Figure 7).

The magnetic properties of the FeCo films were investigated by analyzing the room temperature angular-dependent hysteresis loops collected by sweeping the magnetic field in the range ±0.1 T at different angles ϕ from the [100] MgO direction ($0° < \phi < 180°$, with a 10° step) in the film plane where, due to the shape anisotropy, the magnetization is usually expected to lie. Representative hysteresis loops along the [100], [110], and [010] in-plane MgO crystallographic orientations are shown in Figure 5.

DOI: 10.1021/acsami.5b06030
ACS Appl. Mater. Interfaces 2015, 7, 22341−22347

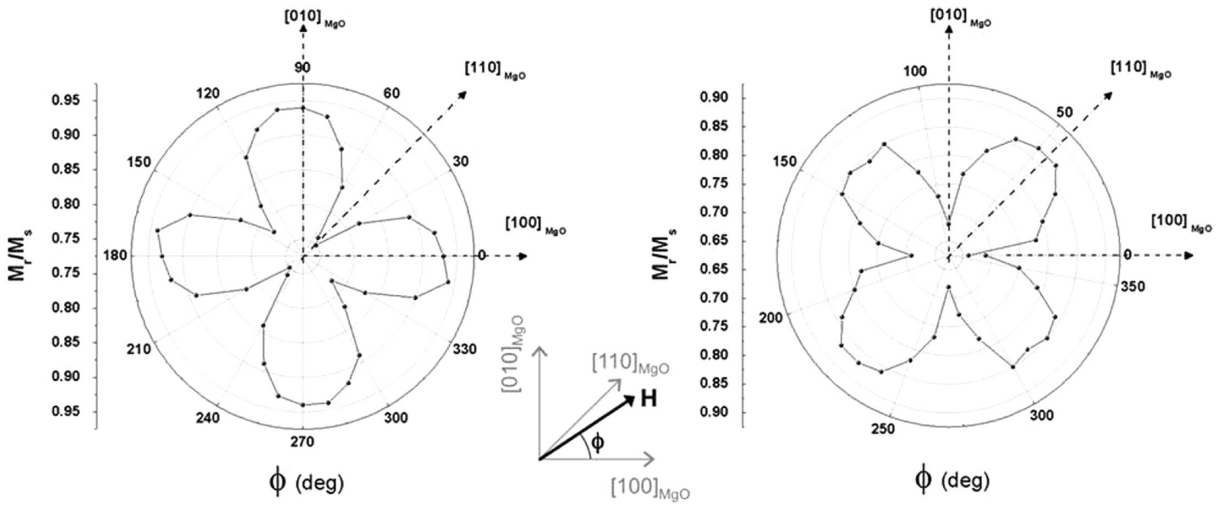

Figure 6. Polar plots of the angular dependence of the reduced remanence magnetization M_r/M_s (ϕ) evaluated from the room temperature angular hysteresis loops ($0° < \phi < 180°$); (left) sample S25, (right) sample S150. The 180−360° branch has been traced by mirroring the 0−180° data.

Both samples showed a magnetization saturation (M_s) of ∼1.88 MA/m that is comparable to the equiatomic $Fe_{50}Co_{50}$ bulk alloy (1.95 MA/m)[2] being also larger than the values commonly reported in the literature, thus confirming the high quality of the films. The change of the hysteresis loop shape with the angle indicates an in-plane anisotropic behavior whose feature is different in the two samples. This aspect is clearly evident in the polar graphs of Figure 6 showing the reduced remanence magnetization M_r/M_s as a function of the field angle ϕ, which exhibits, for both samples, a 4-fold symmetry typical of a cubic system[25,26] with two orthogonal maxima ($M_r/M_s \sim 0.9$) corresponding to the easy magnetization directions at approximately $\phi = \phi_o + n\pi/2$, where $\phi_o = 0$ ($\pi/4$) for sample S25 (S150). The different symmetry reflects a different easy-axes spatial arrangement in the two samples, as discussed below.

DISCUSSION

According to theoretical studies,[27] the nucleation and growth mechanism of laser plasma-deposited thin films can be described as a function of the experimental conditions due to the strict correlation existing between the growth parameters (laser flux density, substrate temperature) and the structural and microstructural film properties. In this work, a high value of laser fluence (7 J/cm^2) was chosen to maximize the deposition rate and to obtain a two-dimensional island growth that takes place when a high number of small nuclei with reduced mobility are quenched on a lower-temperature substrate. It is well-known that the mechanism of formation of the first islands nucleating on the substrate plays the most important role in determining the final morphology and orientation of the film.[28] Moreover, if the surface diffusion is sufficient to allow an island to reach its thermodynamic equilibrium, then its shape and orientation will be determined by the minimization of the total surface free energy. Such energy is composed of three terms: (i) the surface free energy of FeCo islands (γ_{FeCo}) that is minimum for a bcc lattice along the {110} planes (closest packed),[28] (ii) the surface free energy of the substrate, and (iii) the free energy of the interface between the film and the substrate.

However, the deposition conditions do not always allow thermodynamically driven growth, and the dependence of the crystallographic texture on the process parameters may be affected by a combination of both kinetic and thermodynamic aspects. At low substrate temperature, as in the case of sample S25, the high kinetic energy of the adatoms impinging on the substrate does not lead to an extended surface diffusion, and this is expected to limit the achievement of equilibrium in the growth of islands; the growth mechanism is thus governed by the minimization of the interface free energy that is minimized by the reduction of film−substrate mismatch, and a coherent interface is then obtained (Figure 7). The resultant film orientation is the (100) (cube-on-cube growth mode)[29] for which a misfit of ∼4% can be calculated according to the following expression: $100[d(200)_{Mg} - d(110)_{FeCo}]/d(200)_{Mg}$, where $d(ABC)_{XY}$ is the interplanar distance associated with the

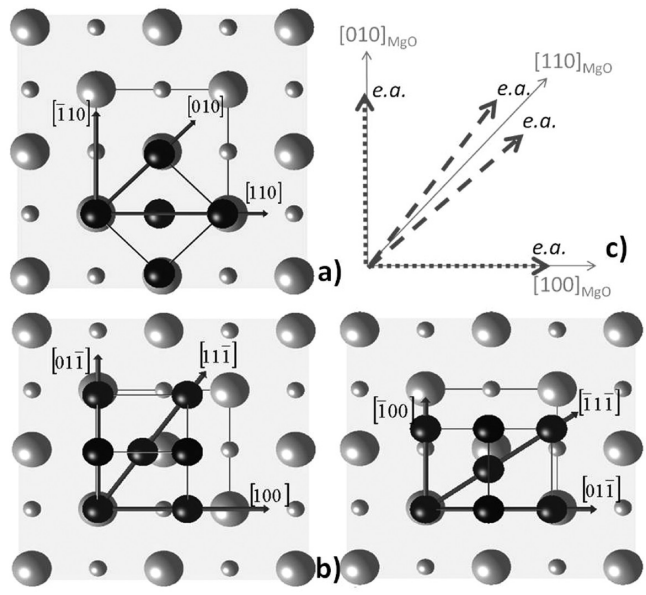

Figure 7. (a,b) In plane growth relationship between the (001) plane of the MgO substrate and the FeCo growth plane: (a) sample S25 (001),[110]FeCo // (001),[100]MgO; (b) sample S150 (011), [100]FeCo // (001),[100]MgO (left) and (011),[011]FeCo // (001),[100]MgO (right). The illustration in (c) indicates the directions of the FeCo magnetocrystalline easy-axis for sample S25 (dotted arrows) and sample S150 (dashed arrows).

DOI: 10.1021/acsami.5b06030
ACS Appl. Mater. Interfaces 2015, 7, 22341−22347

lattice planes (ABC) of the crystallographic phase XY. This value must be compared with that of the S150 sample. In this case, the interception of the FeCo cell on the interface's plane is rectangular; thus, two misfit values can be calculated in two nonequivalent perpendicular directions (Figure 7b). One misfit value is 4%, which is equal to the previous one, whereas the other can be evaluated as $100[d(200)_{Mg} - d(200)_{FeCo}]/d(200)_{Mg} = 32\%$. In this case, with the substrate temperature sufficiently high to promote nuclei diffusion, the cluster coalescence leads to the growth of larger equilibrium islands whose preferential orientation is such as to minimize the total free energy, including the free surface energy γ_{FeCo}. The (110) orientation of sample S150, which is also characterized by larger grains with respect to S25, is consistent with this model. Moreover, the presence of a disordered interface suggests that the γ_{FeCo} term, when not negligible, is higher than the interface energy, and the interfacial layers of the (110)-oriented film relax in a disordered structure.

The in-plane anisotropic magnetic behavior observed in the two samples is consistent with the two different growth orientations of the bcc FeCo films when the magnetocrystalline anisotropy is dominant. For bulk $Fe_{50}Co_{50}$ alloys, the second- and fourth-order magnetocrystalline anisotropy constants are both negative (i.e., $K_1 \approx -7 \times 10^3$ J/m^3 and $K_2 \approx -40 \times 10^3$ J/m^3),[26] from which it results that the easy- and hard-axes would correspond to the [110] and [100] crystallographic directions when the measurements are carried out in the (100) plane (where the contribution of the K_2 constant is zero), and easy-, medium-, and hard-axes are aligned along the [111], [110], and [100] directions, respectively, when the measurements are performed in the (110) plane.[30] This different magnetic behavior is coherently observed in the polar plots reported in Figure 6. For sample S25, the four maxima at $\phi = 0 + n\pi/2$ correspond to the four [110] easy axis directions of the FeCo film. The maximum value of M_r/M_s (~0.9) is slightly smaller than that expected for a perfect cubic crystal (i.e., 1), likely because of a small angular dispersion in the film plane of the [110] crystallographic axis. For sample S150, where two orthogonal FeCo unit cell orientations are possible, the maxima of M_r/M_s, which corresponds to the [111] FeCo crystallographic axis, are tilted approximately ±10° with the respect to the [110] MgO direction (see Figure 7c); this would result, in conjunction with a reasonable slight in-plane angular distribution of the [111] crystallographic axes, in a cone of possible easy-axis directions around the [110] MgO direction. This is experimentally evidenced by the angular remanence curve, where the maximum values are spread to approximately ±10° around $\phi = \pi/4 + n\pi/2$ ($n = 1, 2, \cdots$). The values of the maxima of the reduced remanence (~0.85) are lower than the ones observed in the S25 sample, likely because of larger distribution of the easy axes. It is worth noting that the values of the reduced remanence along the [100] and [110] MgO directions are not different, as expected for an ideal [110] cubic crystal, because of the two possible orthogonal orientations of the FeCo cell that cancels the difference.

The high degree of structural and microstructural ordering is also reflected by the coercivity (H_c) along the easy axis direction, whose values ($\mu_0 H_c$ (S25) ≈ 2 mT and $\mu_0 H_c$ (S150) ≈ 4 mT) are very low compared to typical FeCo thin films deposited at low temperature.[2,31−33] The slight increase of H_c at increasing temperature may be ascribed to an increase in the grain size and/or to the presence of microstructural defects at the interface region that can act as pinning centers that hinder the magnetization reversal during the application of the external field.

CONCLUSIONS

By properly selecting the growth conditions in a PLD process, it possible to obtain FeCo granular thin films characterized by a smooth surface and high degree of crystallographic order with a defined growth orientation that can be suitably varied by changing the deposition temperature ([001] at 25 °C and [110] at 150 °C). The high structural quality, even at room temperature, is reflected in high values of the saturation magnetization (~1.88 MA/m) and low coercivity (~2 mT at 25 °C and ~4 mT at 150 °C, along the easy-axis), matching the requirements for technological applications. The close correlation observed between the anisotropic magnetic behavior and the crystallographic orientation make these samples a model for fundamental studies on magnetic systems characterized by cubic anisotropy.

AUTHOR INFORMATION

Corresponding Author

*E-mail: sara.laureti@ism.cnr.it.

Notes

The authors declare no competing financial interest.

ACKNOWLEDGMENTS

This work was supported by MIUR under project FIRB2010−NANOREST and Ministry of Education and Science of the Russian Federation in the framework of Increase Competitiveness Program of NUST "MISiS".

REFERENCES

(1) Sourmail, T. Near Equiatomic FeCo Alloys: Constitution, Mechanical And Magnetic Properties. *Prog. Mater. Sci.* **2005**, *50* (7), 816−880.

(2) Platt, C. L.; Berkowitz, a. E.; Smith, D. J.; McCartney, M. R. Correlation Of Coercivity And Microstructure Of Thin CoFe Films. *J. Appl. Phys.* **2000**, *88* (4), 2058−2062.

(3) Chappert, C.; Fert, A.; Van Dau, F. N. The Emergence Of Spin Electronics In Data Storage. *Nat. Mater.* **2007**, *6* (11), 813−823.

(4) Ohno, H. A Window On The Future Of Spintronics. *Nat. Mater.* **2010**, *9* (12), 952−954.

(5) Ikeda, S.; Hayakawa, J.; Ashizawa, Y.; Lee, Y. M.; Miura, K.; Hasegawa, H. Tunnel Magnetoresistance Of 604% At 300 K By Suppression Of Ta Diffusion In CoFeB/MgO/CoFeB Pseudo-spin-valves Annealed At High Temperature. *Appl. Phys. Lett.* **2008**, *93*, 2008−2010.

(6) Parkin, S. S. P.; Kaiser, C.; Panchula, A.; Rice, P. M.; Hughes, B.; Samant, M.; Yang, S.-H. Giant Tunnelling Magnetoresistance At Room Temperature With MgO (100) Tunnel Barriers. *Nat. Mater.* **2004**, *3* (12), 862−867.

(7) Ikeda, S.; Miura, K.; Yamamoto, H.; Mizunuma, K.; Gan, H. D.; Endo, M.; Kanai, S.; Hayakawa, J.; Matsukura, F.; Ohno, H. A Perpendicular-anisotropy CoFeB − MgO Magnetic Tunnel Junction. *Nat. Mater.* **2010**, *9* (9), 721−724.

(8) Wang, B.; Oomiya, H.; Arakawa, A.; Hasegawa, T.; Ishio, S. Perpendicular Magnetic Anisotropy And Magnetization of L10 FePt/FeCo Bilayer Films. *J. Appl. Phys.* **2014**, *115* (13), 133908.

(9) Casoli, F.; Albertini, F.; Nasi, L.; Fabbrici, S.; Cabassi, R.; Bolzoni, F.; Bocchi, C. Strong Coercivity Reduction In Perpendicular FePtFe Bilayers Due To Hard/soft Coupling. *Appl. Phys. Lett.* **2008**, *92* (14), 1−4.

(10) Goll, D.; Bublat, T. Large-area Hard Magnetic L1 0 -FePt And Composite L1 0 -FePt Based Nanopatterns. *Phys. Status Solidi A* **2013**, *210* (7), 1261−1271.

DOI: 10.1021/acsami.5b06030
ACS Appl. Mater. Interfaces 2015, 7, 22341−22347

(11) Varvaro, G.; Albertini, F.; Agostinelli, E.; Casoli, F.; Fiorani, D.; Laureti, S.; Lupo, P.; Ranzieri, P.; Astinchap, B.; Testa, A. M. Magnetization Reversal Mechanism In Perpendicular Exchange-coupled Fe/L1 0 − FePt Bilayers. *New J. Phys.* **2012**, *14* (7), 073008.
(12) Burkert, T.; Nordström, L.; Eriksson, O.; Heinonen, O. Giant Magnetic Anisotropy In Tetragonal FeCo Alloys. *Phys. Rev. Lett.* **2004**, *93* (2), 027203−1.
(13) Gong, M.; Kirkeminde, A.; Wuttig, M.; Ren, S. Phase Transformation-Induced Tetragonal FeCo Nanostructures. *Nano Lett.* **2014**, *14*, 10−15.
(14) Díaz-Ortiz, a.; Drautz, R.; Fähnle, M.; Dosch, H.; Sanchez, J. M. Structure And Magnetism In Bcc-based Iron-cobalt Alloys. *Phys. Rev. B: Condens. Matter Mater. Phys.* **2006**, *73* (22), 13−18.
(15) Torchio, R.; Kvashnin, Y. O.; Marini, C.; Mathon, O.; Garbarino, G.; Mezouar, M.; Wright, J. P.; Bruno, P.; Genovese, L.; Baudelet, F.; Meneghini, C.; Mobilio, S.; Morley, N. a.; Gibbs, M. R. J.; Pascarelli, S. Pressure-induced Structural And Magnetic Phase Transitions In Ordered And Disordered Equiatomic FeCo. *Phys. Rev. B: Condens. Matter Mater. Phys.* **2013**, *88*, 1−8.
(16) Aziz, M. J. Film Growth Mechanisms In Pulsed Laser Deposition. *Appl. Phys. A: Mater. Sci. Process.* **2008**, *93* (3), 579−587.
(17) Willmott, P. R. Deposition Of Complex Multielemental Thin Films. *Prog. Surf. Sci.* **2004**, *76*, 163−217.
(18) Martin, L. W.; Chu, Y. H.; Ramesh, R. Advances In The Growth And Characterization Of Magnetic, Ferroelectric, And Multiferroic Oxide Thin Films. *Mater. Sci. Eng., R* **2010**, *68* (4−6), 89−133.
(19) Scavia, G.; Agostinelli, E.; Laureti, S.; Varvaro, G.; Paci, B.; Generosi, A.; Albertini, V. R.; Kaciulis, S.; Mezzi, A. Evolution Of The Pt Layer Deposited On MgO(001) By Pulsed Laser Deposition As A Function Of The Deposition Parameters: A Scanning Tunneling Microscopy And Energy Dispersive X-ray Diffractometry/reflectometry Study. *J. Phys. Chem. B* **2006**, *110* (11), 5529−5536.
(20) Agostinelli, E.; Laureti, S.; Varvaro, G.; Generosi, A.; Paci, B.; Scavia, G.; Testa, A. M. Study Of Structural Microstructural And Magnetic Properties Of Very Thin Co 50 Pt 50 Films Deposited By PLD. *Mater. Sci. Eng., C* **2007**, *27*, 1466−1469.
(21) Laureti, S.; Agostinelli, E.; Fiorani, D.; Generosi, a.; Paci, B.; Rossi Albertini, V.; Testa, a. M.; Varvaro, G. Exchange Bias In Fcc-CoPt/CoO/Si Films As A Function Of Annealing Treatment. *Superlattices Microstruct.* **2009**, *46* (1−2), 90−94.
(22) Shen, J.; Gai, Z.; Kirschner, J. Growth And Magnetism Of Metallic Thin Films And Multilayers By Pulsed-laser Deposition. *Surf. Sci. Rep.* **2004**, *52*, 163.
(23) Meyerheim, H.; Stepanyuk, V.; Klavsyuk, a.; Soyka, E.; Kirschner, J. Structure And Atomic Interactions At The Co/Pd(001) Interface: Surface X-ray Diffraction And Atomic-scale Simulations. *Phys. Rev. B: Condens. Matter Mater. Phys.* **2005**, *72* (11), 10−13.
(24) García-García, A.; Vovk, A.; Pardo, J. a.; Štrichovanec, P.; Maǵn, C.; Snoeck, E.; Algarabel, P. a.; De Teresa, J. M.; Morellón, L.; Ibarra, M. R. Magnetic Properties Of FeMgO Granular Multilayers Prepared By Pulsed Laser Deposition. *J. Appl. Phys.* **2009**, *105* (6), 063909.
(25) Cullity, B. D.; Graham, C. D. *Introducion to Magnetic Materials*, 2nd ed.; John Wiley & Sons: NJ, 2009.
(26) Getzlaff, M. Magnetic Anisotropy Effects. In *Fundamentals of Magnetism*; Springer, 2007; pp 89−115.
(27) Metev, S.; Meteva, K. Nucleation And Growth Of Laser-plasma Deposited Thin Films. *Appl. Surf. Sci.* **1989**, *43*, 402−408.
(28) Feng, Y. C.; Laughlin, D. E.; Lambeth, D. N. Formation Of Crystallographic Texture In Rf Sputter-deposited Cr Thin Films. *J. Appl. Phys.* **1994**, *76* (11), 7311−7316.
(29) Zhao, P.; Huang, Z.; Mao, Y.; Wang, Y.; Takashi, G. Preparation Of (100)-oriented CeO2 Film On (100) MgO Single Crystal Substrate By Laser Chemical Vapor Deposition Using Solid Precursor. *Ceram. Int.* **2014**, *40* (10), 15919−15923.
(30) Cullity, B. D.; Graham, C. D. Introduction To Magnetic Materials. *Introduction to Magnetic Materials* **2009**, 1.
(31) Liu, X.; Kanda, H.; Morisako, A. The Effect Of Underlayers On FeCo Thin Films. *J. Phys. Conf. Ser.* **2011**, *266*, 012037.
(32) Prasanna Kumari, T.; Manivel Raja, M.; Kumar, A.; Srinath, S.; Kamat, S. V. Effect Of Thickness On Structure, Microstructure, Residual Stress And Soft Magnetic Properties Of DC Sputtered Fe65Co35 Soft Magnetic Thin Films. *J. Magn. Magn. Mater.* **2014**, *365*, 93−99.
(33) Vopsaroiu, M.; Georgieva, M.; Grundy, P. J.; Fernandez, G. V.; Manzoor, S.; Thwaites, M. J.; O'Grady, K. Preparation Of High Moment CoFe Films With Controlled Grain Size And Coercivity. *J. Appl. Phys.* **2005**, *97* (10), 10N303.

NOTE ADDED AFTER ASAP PUBLICATION

This paper was published on the Web on October 2, 2015. An additional affiliation was added for Valeria Rodionova, along with additional acknowledgment information. The corrected version was reposted on October 2, 2015.

DOI: 10.1021/acsami.5b06030
ACS Appl. Mater. Interfaces 2015, 7, 22341−22347